Molecular Biology of the Cell
Vol. 21, 970–978, March 15, 2010

Differential Localization and Dynamics of Class I Myosins in the Enterocyte Microvillus

Andrew E. Benesh,* Rajalakshmi Nambiar,* Russell E. McConnell,* Suli Mao,* David L. Tabb,† and Matthew J. Tyska*

*Cell and Developmental Biology Department, and †Department of Biomedical Informatics, Vanderbilt University School of Medicine, Nashville, TN 37205

Submitted July 31, 2009; Revised December 2, 2009; Accepted January 11, 2010
Monitoring Editor: Thomas Pollard

Epithelial cells lining the intestinal tract build an apical array of microvilli known as the brush border. Each microvillus is a cylindrical membrane protrusion that is linked to a supporting actin bundle by myosin-1a (Myo1a). Mice lacking Myo1a demonstrate no overt physiological symptoms, suggesting that other myosins may compensate for the loss of Myo1a in these animals. To investigate changes in the microvillar myosin population that may limit the Myo1a KO phenotype, we performed proteomic analysis on WT and Myo1a KO brush borders. These studies revealed that WT brush borders also contain the short-tailed class I myosin, myosin-1d (Myo1d). Myo1d localizes to the terminal web and striking puncta at the tips of microvilli. In the absence of Myo1a, Myo1d peptide counts increase twofold; this motor also redistributes along the length of microvilli, into compartments normally occupied by Myo1a. FRAP studies demonstrate that Myo1a is less dynamic than Myo1d, providing a mechanistic explanation for the observed differential localization. These data suggest that Myo1d may be the primary compensating class I myosin in the Myo1a KO model; they also suggest that dynamics govern the localization and function of different yet closely related myosins that target common actin structures.

INTRODUCTION

Intestinal epithelial cells lining the small intestine exhibit a remarkably well-organized apical brush border (BB) composed of a tightly packed array of microvilli. Integral to the stability of each microvillus is the core actin bundle and associated actin-binding proteins. Early electron micrographs of microvilli revealed the presence of lateral bridges that connect the microvillar membrane to the underlying actin bundle (Mooseker and Tilney, 1975; Matsudaira and Burgess, 1979). These bridges were later identified as the actin-based motor protein, myosin-1a (Myo1a; Mooseker and Tilney, 1975; Matsudaira and Burgess, 1979; Howe and Mooseker, 1983; Collins and Borysenko, 1984). Because the initial visualization of Myo1a, the list of myosins known to reside in the BB has continued to grow; we now know that representatives from classes I, II, V, VI, and VII target to this actin-rich domain (Heintzelman *et al.*, 1994; Chen *et al.*, 2001). The diversity of myosins in the BB highlights the complexity of this cytoskeletal environment and underscores the need to understand how these myosins interact and function together to contribute to epithelial physiology.

An example of the complex interactions between myosins in the BB was recently provided by cell biological studies of Myo1a, which has been implicated in a wide variety of enterocyte functions ranging from the organization of apical membrane domains (Tyska and Mooseker, 2004) to the control of apical membrane tension (Nambiar *et al.*, 2009) and the shedding of vesicles from the tips of microvilli (McConnell *et al.*, 2009). Indeed, analysis of a Myo1a knockout (KO) mouse revealed defects in BB membrane composition and the presence of apical membrane herniations in a subset of enterocyte BBs (Tyska *et al.*, 2005). Despite these defects, Myo1a KO mice demonstrate no overt physiological symptoms, giving rise to the possibility that other myosins may be able to partially compensate for the absence of Myo1a function in these animals. This idea is supported by more recent studies in isolated BBs, which show that membrane shedding from microvillar tips is significantly reduced, but not abolished in the absence of Myo1a (McConnell and Tyska, 2007). Moreover, immunofluorescence studies do indicate that another short-tailed class I motor, myosin-1c (Myo1c) redistributes from basolateral membranes to the BB in the absence of Myo1a (Tyska *et al.*, 2005). However, Myo1c is only one of seven vertebrate class I myosins that hold the potential to function in place of Myo1a. Although the limited availability of high-quality antibodies restricted the scope of these initial studies, a probe-independent approach, such as proteomic analysis, may provide more comprehensive information on how the absence of Myo1a impacts the complement of motor proteins that reside in the BB.

Here we describe a proteomic approach that led us to identify myosin-1d (Myo1d) as another short-tailed class I myosin in the microvillus. Within wild-type (WT) enterocytes, Myo1d localizes to the basolateral membrane and BB terminal web; Myo1d is also enriched in striking puncta at the distal tips of microvilli. In Myo1a KO mice, Myo1d levels in the BB are increased approximately twofold; this increase is accompanied by a marked redistribution of Myo1d along the length of the microvillus. We also found that in contrast to Myo1a, the microvillar targeting of Myo1d requires both IQ and TH1 (tail homology 1) domains. Finally, fluorescence

This article was published online ahead of print in *MBC in Press* (http://www.molbiolcell.org/cgi/doi/10.1091/mbc.E09–07–0638) on January 20, 2010.

Address correspondence to: Matthew J. Tyska (matthew.tyska@vanderbilt.edu).

recovery after photobleaching (FRAP) studies show that although Myo1d and Myo1a exhibit comparable turnover kinetics in the BB, Myo1a has a significantly larger immobile fraction. In addition to establishing Myo1d as a component of the BB cytoskeleton, these results suggest that dynamics may govern the localization and function of different, yet closely related myosins that target common actin-rich structures. They also highlight the utility of proteomic methods in defining the resident motor proteins that populate specific actin arrays.

MATERIALS AND METHODS

Proteomic Analysis

BBs were isolated from adult mice, killed in accordance with Vanderbilt IACUC protocols. A total of five paired preparations (one preparation included 25 WT and 25 Myo1a KO) were completed for mass spectrometry analysis. Once BBs were collected (described below), total protein concentration was determined using a BCA protein assay kit (Pierce, Rockford, IL). BBs were resuspended in Laemmli loading buffer and separated on a 10% NuPage gel (Invitrogen, Carlsbad, CA). After samples were run into the gel ~2.0 cm, the gel was stained with Coomassie Blue G-250 (Bio-Rad, Richmond, CA) and then destained with sterile milliQ water (Millipore, Billerica, MA). The protein-containing region was excised from the gel and minced with a razor blade (Supplemental Figure 1). Gel fragments were then submitted to Vanderbilt University Mass Spectrometry Core for tryptic digest and subsequent proteomic analysis. Tandem mass spectra were matched to peptide sequences via the MyriMatch algorithm (September, 2007 build; Tabb *et al.*, 2007; Cao *et al.*, 2008). The IPI Mouse 3.33 database provided protein sequences (http://www.ebi.ac.uk/IPI/IPIhelp.html/; Kersey et al., 2004), with each sequence present in both forward and reverse orientations. Variable modifications included oxidation of methionine and loss of ammonia from N-terminal glutamines; all cysteines were considered to be alkylated. IDPicker (Zhang *et al.*, 2007) filtered the raw identifications to a 1% FDR (false discovery rate) and required proteins to feature at least two distinct sequences to be included in the reports. The software also applied a parsimony filter to remove subset and subsumed proteins.

Immunofluorescence

Intestine tissues were dissected and flushed with 37°C Hanks' balanced salt solution (Invitrogen). Three-millimeter fragments of intestine were fixed with 4% paraformaldehyde in PBS (50 mM EGTA, 137 mM NaCl, 7 mM Na_2HPO_4, and 3 mM NaH_2PO_4, pH 7.2) for 30 min at 4°C and then cryoprotected overnight at 4°C in 1 M sucrose in TBS. Samples were embedded into OCT (Sakura Finetek, Torrance, CA), and 10-μm sections were cut using a Leica CM 1900 cryostat (Deerfield, IL). Sections were permeabilized for 1 s with −20°C acetone, and washed with PBS. Next, sections were blocked in 10% BSA/PBS for 20 min and washed. Sections were then incubated with primary antibody targeting Myo1a (4P1, 1:200; developed in our laboratory) and Myo1d (C13, K18, or H60; Santa Cruz Biotechnology, Santa Cruz, CA; 1:50), or intestinal alkaline phosphatase (IAP; Sigma-Aldrich, St. Louis, MO; 1:200) diluted in PBS for 1 h and then washed. Secondary antibodies, donkey anti-goat (Molecular Probes, Eugene, OR; 1:200) and Alexa-conjugated phalloidin (Molecular Probes/Invitrogen, 1:200), were diluted in PBS and applied to sections for 20 min in darkness. Finally, sections were washed three times and prepared for coverslips using ProLong Anti-fade (Molecular Probes/Invitrogen). Samples were viewed on an Olympus FV-1000 with a 100× objective lens (Melville, NY). All images were contrast enhanced, pseudocolored, and cropped with ImageJ v. 1.42h (http://rsb.info.nih.gov/ij/; NIH). BBs were straightened using the ImageJ Straighten Curved Objects plug-in (Eva Kocsis, NIH). After straightening, pixel intensities for red, green, and blue channels were averaged along the axis perpendicular to the microvillar axis using a LabView program developed in-house. Average pixel intensities were then plotted relative to position along the microvillar axis.

Preparation of Whole Cell Homogenates

Intestinal tissues were collected from WT and Myo1a KO mice and placed in ice-cold sucrose dissociation solution (200 mM sucrose, 0.02% Na-azide, 12 mM EDTA-K, 18.9 mM KH_2PO_4, and 78 mM Na_2HPO_4, pH 7.2) for 2 h. Mucosa was scraped from the intestine with a blunt straight-edge and then resuspended in homogenization buffer (10 mM imidazole, 4 mM EDTA-K, 1 mM EGTA-K, 0.02% Na-azide, 1 mM DTT, and 1 mM Pefabloc [Pentapham AG, Basel, Switzerland], pH 7.2).

BB Isolation and Fractionation

BBs were isolated from mouse small intestinal tissues as previously described (Tyska *et al.*, 2005). For biochemical extraction, isolated BB pellets were first treated with 1% NP-40 in buffer A′ (75 mM KCl, 20 mM imidazole, 1 mM EGTA, 2.5 mM $MgCl_2$, 0.02% Na-azide, 1 mM DTT, and 1 mM Pefabloc pH 7.2) for 5 min on ice. Samples were then centrifuged at 5000 × *g* for 10 min. The resulting pellet was washed twice in A′ with 10-min spins at 5000 × *g*. Detergent extracted BBs were then treated with 2 mM ATP in A′ and quickly sedimented at 10,000 × *g* for 10 min at 4°C. The resulting supernatant was collected and then centrifuged at 100K × *g* for 1 h at 4°C (Beckman Instruments, Fullerton, CA; TL-100 ultracentrifuge). The 100K × *g* pellet was resuspended in a volume of A′ equivalent to the supernatant.

Immunoblotting

Primary antibodies used for immunoblotting were diluted to 1:1000, including Myo1a (4P1, developed by our laboratory), enhanced green fluorescent protein (EGFP; Molecular Probes, A11122) and nonmuscle Myo2 (Biomedical Technologies, Stoughton, MA). H60 (Santa Cruz Biotechnology) and antibody 482 which targets amino acids 991-1006 of Myo1d were both used at 1:500 (a gift from Martin Bahler, Westfälische Wilhelms-Universität Münster, Münster, Germany; Huber *et al.*, 2000). Secondary antibodies included fluorescent IRDye800-conjugated donkey anti-rabbit IgG (Li-Cor Biosciences, Lincoln, NE) and fluorescent-conjugated Alexa 680 donkey anti-goat IgG (Molecular Probes). Blots were processed according to manufacturer's recommendations and scanned on an Odyssey Imager (Li-Cor). For some biochemical experiments, the secondary antibody was HRP-conjugated goat anti-rabbit IgG, in these cases, immunogens were imaged with ECL reagents according to the manufacturers recommendations (GE Healthcare, Waukesha, WI).

Molecular Cloning

A full-length *Rattus norvegicus* Myo1d clone (IMAGE I.D. 7106587) was obtained from the Mammalian Gene Collection (http://mgc.nci.nih.gov/). Conventional PCR cloning was used to insert the Myo1d coding sequence into pEGFP-C1 (Clontech, Palo Alto, CA) with a forward primer containing a SacI site (AATTGAGCTCGCGCCATGGCGGAGCAGGAGAG) and a reverse primer with a BamHI site (TGTTGGATCCTCAATTCCCGGGCACACTGA). Myo1d Motor (nucleotides 1–2109) was cloned into the pmCherry-N3 vector with the same forward primer as above and a reverse primer with a BamHI site (TGGTGGATCCGAGGACAACCCTGACGAGCATC). Myo1d-MotorIQ (nucleotides 1–2217) was cloned into the pmCherry-N3 vector with the same forward primer as above and a reverse primer containing a BamHI site (GGTTGGATCCGTACGACTTCACTTTATAGC). Myo1d IQ-TH1 (nucleotides 1708–3018) was inserted into the EGFP-C1 vector using the EcoRI and SacI sites. The Myo1d TH1 domain (nucleotides 2242–3018) was cloned into the EGFP-C1 vector using a forward primer containing a SacI site (GCGAGCTCACGGGGTCAAGA) and the same reverse primer as above. The Myo1d IQ domain (nucleotides 2082–2241) was cloned into the EGFP-C1 vector using a forward primer containing an EcoRI site (CGGCGGATCCGAATCGCCTGGCTACCTCGTG) and a reverse primer containing a BamHI site (CTACGAATTCCATCGCGCCCAGATGCTCGTCAGG).

Cell Culture

LLC-PK1-CL4 cells were cultured in Alpha minimum essential medium (Invitrogen), 10% defined fetal bovine serum (HyClone, Logan, UT), and 2 mM L-glutamine (Invitrogen). Cells were incubated at 37°C and 5% CO_2. LLC-PK1-CL4 cells were transfected using Lipofectamine 2000 (Invitrogen) according to the manufacturer's protocols.

Fluorescence Recovery after Photobleaching

FRAP was performed as previously described (Tyska and Mooseker, 2002). Briefly, LLC-PK1-CL4 cells stably expressing EGFP-Myo1d or EGFP-Myo1a were grown to confluency on MatTek (Ashland, MA) 35-mm glass-bottomed dishes. Before imaging, complete medium was exchanged for 25 mM HEPES-buffered DMEM lacking phenol red, and mineral oil was layered on top to prevent medium evaporation. Cells were incubated in a WeatherStation (Precision Control, Sammamish, WA; http://www.precisioncontrol.net/) at 37°C and imaged using an Olympus FV-1000 laser scanning confocal microscope. A field of 105.6 × 105.6 μm was scanned every 3 s, and a region of interest (ROI) for photobleaching was set at 5 μm^2. Bleaching was performed with three scans at 100% transmission. Immediately after bleaching, the entire field was scanned at 3-s intervals. ImageJ was used to extract the ROI integrated pixel intensities from raw data files; intensity data were then exported to a Microsoft Excel (Redmond, WA) where background and $t = 0$ intensity values were subtracted from each time point. Intensity data were normalized so that the scan immediately before photobleaching was equal to 1. Using SigmaPlot (v.10; Systat, San Jose, CA) recovery data were fit to the following kinetic model: $I_{ROI}\ (t \geq 0) = \alpha - A_{1exp}{}^{-k1t} - A_{2exp}{}^{-k2t}$, where I_{ROI} is the ROI intensity at time $t \geq 0$, α is the mobile fraction and A_x is the amplitude of the exponential process with rate k_x.

RESULTS

Four Class I Myosins Reside in the Mouse Enterocyte BB

To identify class I myosin proteins that may be compensating for the loss of Myo1a in KO BBs, we submitted five

Table 1. Proteomic analysis of class I myosins in the enterocyte BB

Protein	IPI identifier	WT total[a]	KO total[a]	% change
Myo1a	IPI00465712.5	1068	3	−99.7
Myo1c	IPI00620222.2	19	25	31.6
Myo1d	IPI00408207.2	171	395	131.0
Myo1e	IPI00330649.4	6	11	83.3
Calmodulin	IPI00467841.6	8	3	−62.5
Nm Myo2c	IPI00453996.1	1796	1801	0.3

[a] Total spectra obtained in the analysis of five paired WT and Myo1a KO BB preparations; see Supplemental Methods for details.

paired preparations of BBs isolated from adult WT and KO mice for proteomic analysis with two-dimensional liquid chromatography tandem mass spectrometry (2D-LC-MS/MS). Resulting mass spectra were assigned to peptides with MyriMatch, a database search algorithm employing multivariate hypergeometric analysis (Tabb *et al.*, 2007). Peptides were then assigned to proteins using IDPicker, a parsimony-based protein assembly tool (Zhang *et al.*, 2007). The peptide counts reported here represent the total number of peptides assigned to a given myosin from all five BB preparations (Table 1). Although this shotgun proteomic approach does not allow for a rigorous quantification of protein levels in our samples, relative comparisons between genotypes are possible because equal amounts of total protein were subject to 2D-LC-MS/MS. Indeed, the number of peptides obtained for nonmuscle myosin-2 (nm Myo2c), a protein not expected to change in KO BBs (Tyska *et al.*, 2005), was nearly identical between genotypes. In contrast, the number of detectable calmodulin peptides decreased in KO samples, consistent with earlier findings (Tyska *et al.*, 2005).

Proteomic analysis of the BB detected four class I myosins: Myo1a, Myo1c, Myo1d, and Myo1e. Three of these four identifications have been reported in previous studies (Tyska *et al.*, 2005). Consistent with immunofluorescence observations showing the redistribution of Myo1c into the BB in the absence of Myo1a (Tyska *et al.*, 2005), we observed a ~30% increase in the number of Myo1c peptides detected in Myo1a KO samples. However, the presence of high levels of Myo1d in WT BBs was an unexpected result. In addition, Myo1d peptide counts increased ~130% in the absence of Myo1a. These data show that Myo1d is a constituent of the BB under normal circumstances and the principal class I myosin in BBs lacking Myo1a.

Myo1d Localizes to the BB Terminal Web and Microvillar Tips

Given that Myo1d has not been previously observed in the vertebrate BB, we sought to validate our proteomics data with conventional cell biological methods. To examine Myo1d localization in the enterocyte, we stained sections of mouse small intestine with a commercially available antibody (C13; Santa Cruz Biotechnology). This anti-Myo1d probe targeted the enterocyte basolateral membrane as well as the terminal web of the BB (Figure 1A), a cytoskeletal meshwork at the base of microvilli that consists of the actin bundle rootlets, spectrin, nm Myo2, interwoven with an array of intermediate filaments (Mooseker, 1985). The observed C13 terminal web staining was a consistent feature along the full length of villi throughout the small intestine. Strikingly, the C13 probe also labeled a population of discrete Myo1d puncta at the distal ends of microvilli (Figure 1B). Phalloidin labeling revealed that Myo1d puncta appear at the distal tips of core actin bundles (Figure 1B, inset). Close examination of frozen sections revealed that C13 labeled microvillar tips mostly along the distal half of the villus.

Interestingly, when two other commercially available Myo1d antibodies (K18 and H60) were applied to sections of small intestine, these antibodies each targeted a distinct subcellular Myo1d population. The K18 antibody targeted Myo1d at microvillar tips, whereas the H60 antibody targeted the terminal web and basolateral membrane (Supplemental Figure 2). Thus, the C13 staining described above (Figure 1) represents a composite of the labeling patterns produced by these two probes. The different patterns observed here are likely related to the fact that these probes target distinct C-terminal epitopes of Myo1d, which may be differentially masked or exposed in different regions of the enterocyte.

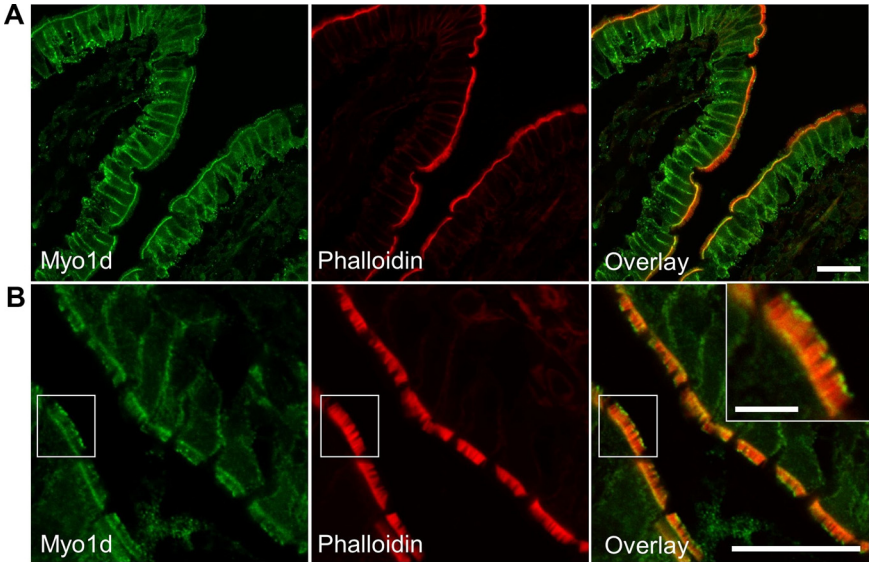

Figure 1. Myo1d localizes to the enterocyte basolateral membrane, terminal web, and microvillar tips. Representative frozen sections of mouse small intestine stained with antibodies targeting Myo1d (green) and Alexa 488 (or 633)–conjugated phalloidin (red). (A and B) Myo1d C13 antibody targets the basolateral membrane, terminal web, and microvillar tips of enterocytes. Bar, 20 μm; inset bar, 5 μm.

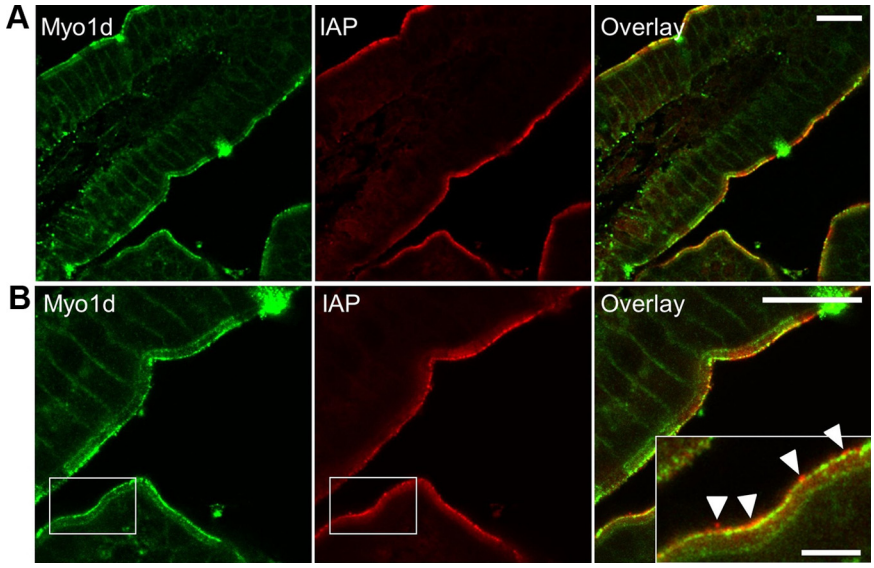

Figure 2. Myo1d and IAP partially colocalize at tips of microvilli. Frozen sections of mouse small intestine labeled with antibodies targeting Myo1d (green) and IAP (red). (A) Confocal image of a villus demonstrating both Myo1d and IAP localize to microvillar tips. (B) Representative view of partial colocalization between Myo1d and IAP at microvillar tips. Myo1d at microvillar tips appears in two populations: alone in distinct puncta, and colocalized with IAP. Arrowheads mark IAP-enriched puncta that lack Myo1d at the extreme distal tips of microvilli. Bars, (A and B) 20 μm; inset in B, 5 μm.

Myo1d Partially Colocalizes with IAP at Microvillar Tips

Recent studies have revealed that enterocyte microvilli release small vesicles enriched in IAP from their distal tips (McConnell *et al.*, 2009). These previous experiments also showed that IAP is enriched in discrete puncta at microvillar tips, presumably intermediates in the vesicle formation and release pathway. To determine if Myo1d is present in these puncta, we double-stained intestinal frozen sections for Myo1d and IAP. Confocal imaging revealed bright regions of IAP staining at microvillar tips as previously reported (Figure 2). Although Myo1d tip labeling was readily observed, only a subset of the Myo1d signal at microvillar tips colocalized with IAP-enriched puncta. In some regions, IAP enriched puncta were observed at more distal positions than Myo1d (arrowheads, Figure 2B, inset), giving rise to the possibility that vesicles released into the lumen may not be enriched in this motor. This is consistent with our previous proteomic analysis of microvillus-derived vesicles (McConnell *et al.*, 2009), which identified a total of three Myo1d peptides in two out of three preparations (unpublished data). Together these data suggest that Myo1d may play a role in the early stages of vesicle formation at microvillar tips, but is not included as "cargo" in vesicles that are ultimately released into the intestinal lumen.

Subcellular Fractionation of Myo1d Is Altered in the Absence of Myo1a

As a first step toward understanding how Myo1d responds to the absence of Myo1a, we examined whole cell levels of Myo1d in WT and Myo1a KO enterocytes. Western blots of mucosal scrapings show that total cellular levels of Myo1d are unaltered in KO animals (Figure 3A). This suggests that the increase in peptide counts observed in our proteomic analysis is likely the result of a redistribution of the Myo1d population normally expressed in enterocytes. To further investigate this possibility, isolated BBs were biochemically extracted using detergent and ATP. BBs were first exposed to 1% NP-40 to release detergent-soluble membranes (DSMs). As expected, neither Myo1a nor Myo1d were released from the BB by detergent treatment (Figure 3B). Next, the NP-40–insoluble fraction was treated with 2 mM ATP to release myosin motors and bound cargoes such as detergent-resistant membranes (DRMs, +ATP, S in Figure 3B), from core actin bundles (+ATP, P in Figure 3B). In WT BBs, almost all of the Myo1d solubilized with ATP treatment, whereas Myo1a distributed equally between ATP soluble and insoluble fractions. Thus, in the presence of ATP, Myo1a may have a greater affinity for actin than does Myo1d. This finding may help explain why Myo1a effectively prevents Myo1d from targeting along the length of microvillar actin bundles in WT BBs. In Myo1a KO BBs, the amount of Myo1d associated with core actin bundles after ATP treatment increased dramatically (+ATP, P in Figure 3B).

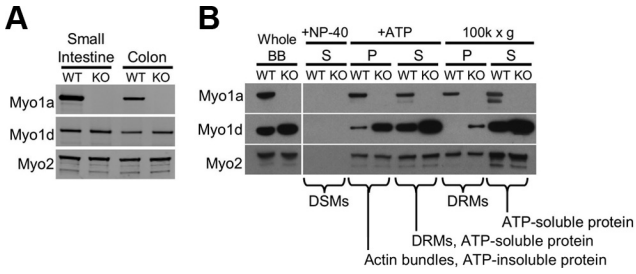

Figure 3. Myo1d redistributes within the enterocyte in the absence of Myo1a. (A) Whole cell lysates were created from WT and KO small intestine and colon mucosal scrapings and then blotted for Myo1a and Myo1d. (B) Compartmentalization of Myo1d within the BB is Myo1a-dependent. Myo1d protein levels are slightly higher in KO BBs compared with WT BBs. Neither Myo1d nor Myo1a are found with detergent-solubilized membranes (DSMs) from whole BBs after treatment with 1% NP-40 (+NP-40, S). On treatment with mM ATP, Myo1a distributes equally between soluble (+ATP, S) and insoluble (+ATP, P) fractions. Most Myo1d is found in the supernatant, with low levels remaining in the pellet. In the absence of Myo1a, the amount of Myo1d associated with actin bundles increases dramatically. Centrifugation of the ATP supernatant (+ATP, S) at 100K $\times$ *g* enables the separation of DRMs (100K $\times$ *g*, P) from purely soluble proteins (100K $\times$ *g*, S). In WT samples, Myo1a partitions equally between the DRM and soluble fractions, whereas Myo1d does not sediment with DRMs. However, Myo1d signal appears in the DRM-enriched 100K $\times$ *g* pellet in Myo1a KO samples. The 100K $\times$ *g* gel samples were concentrated 2.5-fold relative to all other samples. Because Myo2 is a BB component that is not expected to change in the absence of Myo1a (see Table 1), blots for Myo2 are shown as a loading control.

The supernatant created after ATP treatment (+ATP, S in Figure 3B) contains soluble myosins, such as Myo1a, and Myo1a-associated cargoes including DRMs (Tyska and Mooseker, 2004). To determine if Myo1d also interacts with DRMs, these membranes were sedimented from the ATP-soluble fraction using ultraspeed sedimentation (100K × *g*, 1 h). In WT samples, Myo1a was found in both the DRM (100K × *g*, P in Figure 3B) and soluble protein (100K × *g*, S in Figure 3B) fractions, whereas Myo1d was strictly soluble. In Myo1a KO samples, however, Myo1d was detectable in the DRM-containing 100K × *g* pellet (100K × *g*, P in Figure 3B). Together these fractionation studies suggest that in KO enterocytes, the BB population of Myo1d reorganizes to occupy compartments that are normally only occupied my Myo1a (e.g., actin bundles and DRMs).

Myo1d Redistributes Along the Length of Microvilli in the Absence of Myo1a

To further explore the nature of Myo1d redistribution throughout the BB in the absence of Myo1a, we stained frozen sections of WT and Myo1a KO small intestine with antibodies directed against both motors. Similar to previous reports (Heintzelman *et al.*, 1994; Skowron and Mooseker, 1999; Tyska *et al.*, 2005), Myo1a demonstrated uniform signal along the length of the microvillus (Figure 4A). However, the populations of Myo1d at the terminal web and tips of microvilli did not exhibit observable overlap with Myo1a. Indeed, high-resolution confocal micrographs revealed that Myo1a was actually excluded from the distal tip compartment occupied by Myo1d (Figure 4A, inset). Quantification of fluorescence (Supplementary Figure 3) revealed that the Myo1a signal begins just distal to the terminal web and parallels the phalloidin signal along the microvillar axis (red line, Figure 4C). However, the Myo1d signal peaks in two regions that flank the phalloidin signal, corresponding to the terminal web and microvillar tips, respectively (green line, Figure 4C). The distinct distributions observed here suggest that even closely related short-tailed class I myosins may be responsible for distinct functions within the microvillus.

Intriguingly, in the absence of Myo1a, Myo1d demonstrated prominent staining along the length of microvilli (Figure 4, B and D), a result consistent with the biochemical fractionation data presented above (Figure 3B). Both terminal web and basolateral membrane labeling in the KO enterocytes were significantly reduced relative to WT samples (Figure 4B, Supplemental Figure 4), suggesting that Myo1d signal along the length of microvilli in KO BBs appears at the expense of these two populations. In contrast to the terminal web and basolateral populations, distinct microvillar tip labeling was still observed, indicating that Myo1d targets to this compartment independent of Myo1a levels in the BB (Figure 4, B and D).

In combination, these data reveal that outside of the microvillar tip compartment, the subcellular localization of Myo1d depends on the level of Myo1a present in the BB. Moreover, by showing that Myo1d redistributes along the length of microvilli in the absence of Myo1a, these results also demonstrate that Myo1d is well positioned to compensate for lost Myo1a function in the KO BBs.

Myo1d Targeting to the BB Requires Both IQ and TH1 Domains

In order for Myo1d to fulfill functions normally carried out by Myo1a, one would expect this motor to target to the apical membrane using a mechanism similar to Myo1a. Previous work has shown that the TH1 domain

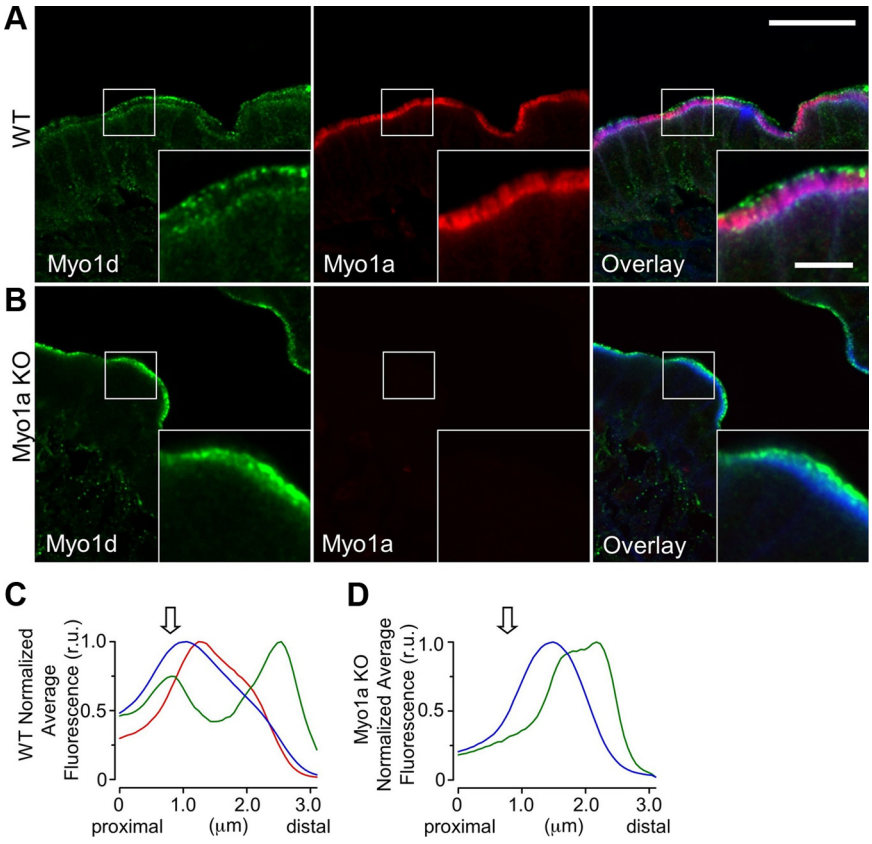

Figure 4. Myo1a and Myo1d exhibit differential localization within the BB. (A) Confocal images of adult WT mouse small intestine frozen sections stained for Myo1d (green, C13 antibody), Myo1a (red), and F-actin (blue). In the BB, Myo1d occupies microvillar tips and the terminal web, whereas Myo1a localizes along the length of microvilli. (B) KO mouse sections stained in an identical manner reveal that Myo1d is found along the length of microvilli in the absence of Myo1a. Myo1d still occupies microvillar tips, but redistributes from lateral plasma membrane and the terminal web. (C and D) Plots show the average pixel intensity along the microvillar axis from proximal (base) to distal (tip) for Myo1d (green), Myo1a (red), and phalloidin (blue) fluorescence signals. The arrow indicates the position of the terminal web. Representative micrographs of "straightened" BBs used to create these plots are shown in Supplemental Figure 3. Bar, 20 μm; inset bar, 5 μm; bars serve as calibration for A and B.

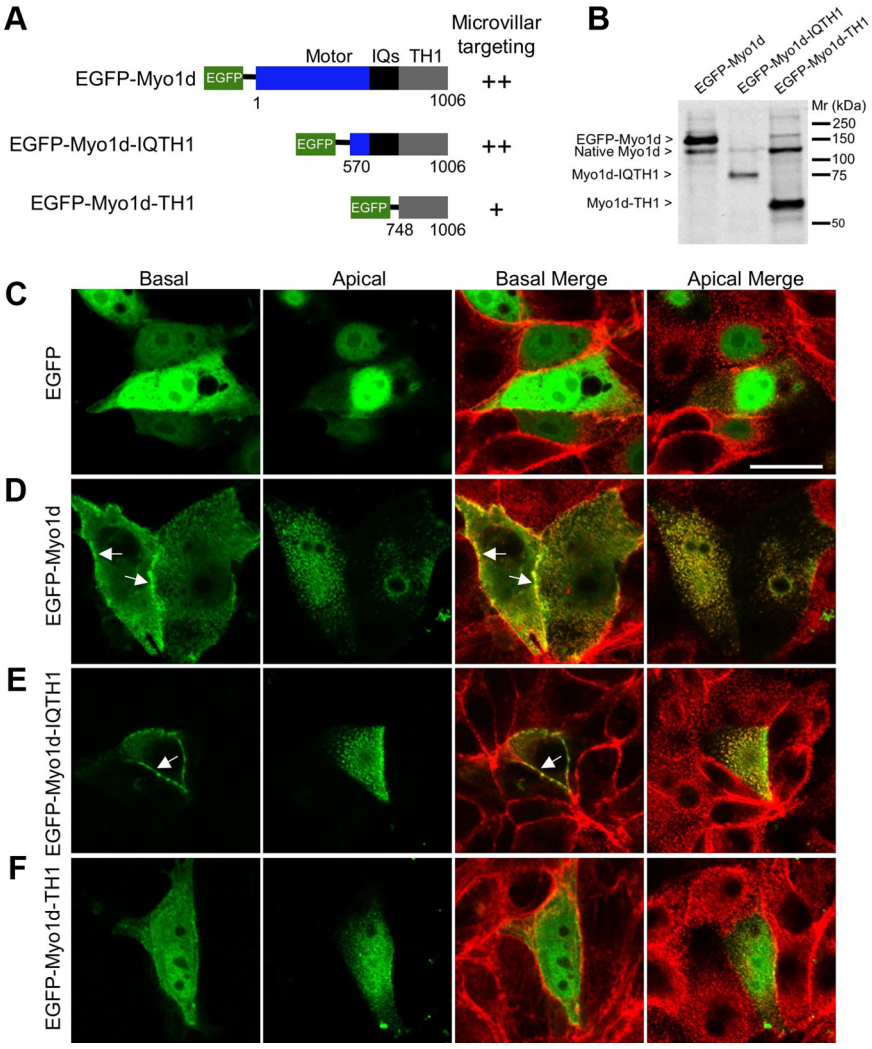

Figure 5. Truncation analysis reveals that both IQ and TH1 domains are needed for proper localization of Myo1d. (A) Diagram of constructs that were generated for studying Myo1d localization determinants. EGFP was fused to the N-terminus of the full-length molecule, Myo1d-IQTH1, or Myo1d-TH1. An indication of the ability of each construct to target to microvilli is provided to the right of the diagram. (B) Western blots with the H60 anti-Myo1d antibody confirm that fragments of the expected size are produced in CL4 cells. (C–F) Confocal micrographs of CL4 cells expressing one of three EGFP-tagged Myo1d constructs or EGFP alone (green) and counterstained with Alexa 488– or Alexa 633–conjugated phalloidin (red). Merges of green and red channels are shown at both apical and basal planes. (C) EGFP alone demonstrates diffuse localization throughout the cytosol and nucleus. (D) EGFP-Myo1d is enriched in microvilli and also targets the lateral plasma membrane, in a manner similar to that previously reported for EGFP-Myo1a (Tyska and Mooseker, 2002). (E) EGFP-Myo1d-IQTH1 localizes to microvilli and lateral membranes in a manner similar to full-length Myo1d. (F) EGFP-Myo1d-TH1 demonstrates low level targeting to microvilli and plasma membrane. Bar, (A) 20 μm (serves as a calibration for A–E).

alone is sufficient for Myo1a localization to microvilli (Tyska and Mooseker, 2002). To investigate which domains are required for Myo1d localization, we expressed truncated EGFP-tagged forms of Myo1d and analyzed their subcellular distribution. Constructs consisting of EGFP fused to different portions of Myo1d (Myo1d, aa 1-1006; Myo1d-IQTH1, aa 570-1006; Myo1d-TH1, aa 748-1006 (Figure 5, A and B); Myo1d-Motor, aa 1-703; Myo1d-MotorIQ, aa 1-739, and Myo1d-IQ, aa 694-747 (Supplemental Figure 5A) were expressed in LLC-PK1-CL4 (CL4) cells and their ability to localize to the plasma membrane and specifically, apical microvilli were examined using confocal microscopy. Consistent with endogenous staining (Figure 1), full-length Myo1d localized to both microvilli and the basolateral membrane (Figure 5D). Myo1d-IQTH1 also localized to microvilli and the basolateral membrane, similar to the full-length construct (Figure 5E). However, the Myo1d-TH1 domain alone appeared mostly cytosolic with weak targeting to microvilli (Figure 5F). Finally, Myo1d-Motor, Myo1d-MotorIQ, and Myo1d-IQ domains failed to exhibit proper targeting (Supplemental Figure 5). These experiments show that although both IQ and TH1 domains appear to be necessary, neither is sufficient for the proper targeting of Myo1d.

FRAP Reveals That Myo1a Is Less Dynamic than Myo1d

The altered Myo1d distribution in Myo1a KO BBs suggests that these two class I myosins may compete for shared binding sites (e.g., membrane receptors) within the microvillus. From this perspective, the nonoverlapping distributions of Myo1d and Myo1a observed in WT enterocytes could be explained by differential dynamics within the BB. For example, Myo1a may exhibit slower turnover rates or a larger immobile fraction relative to Myo1d, making it difficult for the latter to occupy common binding sites along the length of the microvillus. To test this model, we performed FRAP analysis on CL4 cells expressing EGFP-Myo1d or EGFP-Myo1a to measure turnover kinetics in this BB model system (Tyska and Mooseker, 2002). CL4 cells express very low levels of both Myo1a and Myo1d (only detectable via Western blot) and thus provide a convenient opportunity to examine the dynamics of these two motors independent of one another, but in the same cellular background. For these experiments, we used a laser scanning confocal microscope to photobleach a region (5 μm^2) in the focal plane of microvilli (Figure 6, A and B). FRAP recovery data were fit to a general kinetic model that assumes that the mobile population consists of two components: a fast population that represents freely diffusing protein and a second slower pop-

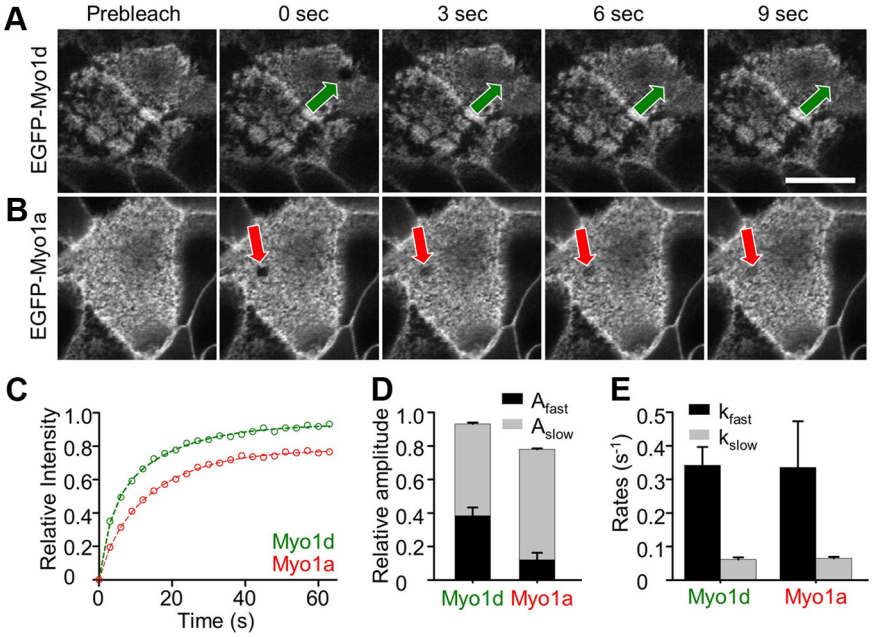

Figure 6. Myo1a and Myo1d demonstrate differential dynamics in the BB. (A) EGFP-Myo1d and (B) EGFP-Myo1a were expressed in CL4 cells and grown on filters for FRAP studies. Micrographs show representative examples of photobleaching; ROIs are marked with an arrow. (C) Averaged datasets (n = 14 for EGFP-Myo1a, n = 22 for EGFP-Myo1d) of the relative fluorescence recovery in photobleached regions were fit to a general kinetic model as outlined in Methods. Myo1d (green) demonstrates more complete recovery (i.e., a higher mobile fraction) when compared with Myo1a (red). (D) Stacked bar graphs of the amplitudes for Myo1d and Myo1a (Fast phase, black; Slow phase, gray). (E) Bar graphs of the rate constants for Myo1d and Myo1a (Fast phase, black; Slow phase, gray). Bar, (A) 20 μm (serves as a calibration for A and B).

ulation that represents protein interacting with BB components (Figure 6C; Tyska and Mooseker, 2002). Interestingly, the fast mobile components measured for Myo1a and Myo1d were nearly identical at ~0.34 s^{-1}; recovery rates for the slow mobile components were also similar at ~0.06 s^{-1} (Figure 6E). However, significant differences were observed in the total mobile fractions for Myo1a and Myo1d, 0.78 versus 0.93, respectively (Figure 6, C and D; Table 2). Fits to the data indicate that the differences in mobile fraction are accompanied by different amplitudes for the fast and slow mobile components. Myo1a demonstrated a very low ratio of fast-to-slow amplitudes (A_{fast}/A_{slow} = 0.18), whereas Myo1d demonstrated a much higher ratio (A_{fast}/A_{slow} = 0.69; Figure 6D, Table 2). Thus, although Myo1a and Myo1d demonstrate comparable turnover kinetics in the BB, Myo1a appears to have a significantly larger immobile fraction (i.e., a lower mobile fraction) on the time scale of these FRAP measurements (~1 min). These results suggest that differences in dynamics may help explain how similar motor molecules can display distinct subcellular localizations within the same organelle.

DISCUSSION

Multiple Class I Myosins in the Microvillus

In this study, we exploit an unbiased shotgun proteomic approach to examine the complement of class I myosins that reside in the vertebrate BB; we also explore how this complement changes in the absence of the major BB component, Myo1a. Four class I myosins were identified in our analysis: Myo1a, Myo1d, Myo1c, and Myo1e (listed in order of decreasing peptide counts). In addition to Myo1a, previous studies have reported the presence of Myo1c and Myo1e in the apical domain of the enterocyte (Skowron *et al.*, 1998; Tyska *et al.*, 2005). Early studies demonstrated the presence of Myo1d transcripts in vertebrate small intestine (Bahler *et al.*, 1994), yet the high levels of Myo1d in the BB and its unique localization at the tips of microvilli were unexpected. Although Myo1d was abundant in WT BBs, peptide counts increased ~2.3-fold in Myo1a KO samples, the most robust change observed for any of the myosin Is detected in this analysis. These data suggest that Myo1d is a component of the microvillus under normal conditions and is the motor most likely to recover functions that are compromised in the absence of Myo1a.

Myo1a-dependent Targeting of Myo1d in the Microvillus

Studies presented here show that Myo1d localization in the BB and its distribution along the microvillus are strongly influenced by the high levels of Myo1a that are normally expressed in the enterocyte. We propose that the differential localization and dynamics observed for Myo1a and Myo1d are the result of differences in the binding affinities that these motors exhibit for microvillar components. For example, when BB fractions are exposed to millimolar levels of ATP, almost all of the Myo1d is released, whereas only ~50% of

Table 2. Summary of FRAP kinetic data

Construct	A_{fast}	k_{fast} (s^{-1})	A_{slow}	k_{slow} (s^{-1})	A_{fast}/A_{slow}	Mobile fraction (α)
EGFP-Myo1a (n = 14)	0.12 ± 0.04	0.34 ± 0.14	0.66 ± 0.04	0.06 ± 0.01	0.18	0.78 ± 0.01
EGFP-Myo1d (n = 22)	0.38 ± 0.05	0.34 ± 0.05	0.55 ± 0.04	0.06 ± 0.01	0.69	0.93 ± 0.01

Photobleaching recovery curves were fit to a kinetic model as described in *Materials and Methods.* Values listed here represent fit parameters ± SE of the fit; A_x, amplitude for process x; k_x, rate for process x; and n, number of BBs sampled.

the Myo1a is solubilized (Figure 3B). This indicates that Myo1a has a higher affinity for actin in the presence of ATP. In addition, the amount of Myo1d found in actin bundle–containing fractions increases markedly in the absence of Myo1a (+ATP, P; Figure 3B). Higher affinities for actin would enable Myo1a to out-compete Myo1d for binding sites along the microvillus length. This model becomes even more attractive if one turns to the proteomics data to gain insight on the relative abundance of these motors in the microvillus. Based on the number of peptides detected in each case, Myo1a is about fivefold more abundant than Myo1d. Thus, the total number of Myo1d molecules in the BB demonstrate ~1:1 stoichiometry with the "immobile" population of Myo1a molecules (~20% of the total).

Function of Myo1d in WT BBs

The unique punctate localization pattern of Myo1d at microvillar tips and prominent banding at the terminal web implies that this motor may be carrying out distinct functions at these locations. Myo1d located in the terminal web may play a role in the short-range transport, docking, and/or fusion of apically directed vesicles derived from the Golgi complex (Fath and Burgess, 1993). Indeed, previous Myo1d studies have shown that this motor associates with vesicle populations in neurons (Bahler *et al.*, 1994) and in early endosomal vesicles in MDCK cells (Huber *et al.*, 2000), supporting a role in trafficking. More recently, Myo1d was implicated in left-right asymmetrical gut patterning during *Drosophila* development (Hozumi *et al.*, 2006; Speder *et al.*, 2006), although the implications for Myo1d function in the vertebrate gut have not been explored.

One of the most striking findings of the current study was the punctate Myo1d staining observed at the tips of microvilli. Early electron micrographs of BB microvilli revealed a dense tip complex at the distal end of core actin bundles (Mooseker and Tilney, 1975), yet the composition of this complex remains poorly characterized. Although Eps8 has been localized to microvillar tips in *Caenorhabditis elegans* (Croce *et al.*, 2004), to our knowledge, Myo1d is the first motor protein shown to target to the distal tip compartment in these structures. Although myosin-7b localizes to the distal half of microvilli (Chen *et al.*, 2001) and myosin-5 exhibits distal microvillar localization (Heintzelman *et al.*, 1994), neither myosin clearly exhibits the punctate localization at microvillar tips displayed by Myo1d. The tip localization described here is reminiscent of myosin-10 accumulation at filopodia tips, where it regulates the formation of these dynamic protrusions (Berg and Cheney, 2002). In the stereocilium, another parallel actin bundle supported protrusion, myosin-3a localizes espin to the stereocilia tip where it plays a critical role in regulating stereocilia length (Les Erickson *et al.*, 2003; Schneider *et al.*, 2006; Salles *et al.*, 2009). Myosin-15a also localizes to stereocilia tips (Belyantseva *et al.*, 2003) and has been implicated in the tip-ward transport of whirlin (Belyantseva *et al.*, 2005). Thus, Myo1d at the tips of microvilli may function in the control of actin bundle dynamics or perhaps the transport of components along the microvillar axis. Alternatively, Myo1d could play a role in the formation and/or release of vesicles from microvillar tips (McConnell and Tyska, 2007), as suggested by the partial colocalization with IAP at the distal ends of microvilli.

Myo1d Function in the Absence of Myo1a

Although the TH1 domains of Myo1d and Myo1a only share 22.2% identity, they are both enriched in basic residues that are required to properly target both Myo1a (Tyska and Mooseker, 2002) and Myo1d to microvilli. This shared feature may allow these two molecules to bind similar protein and/or lipid targets and engage in similar functions. In the vertebrate BB, Myo1a forms bridges that link the actin core bundle and plasma membrane, suggesting that this molecule may play a role in maintaining the structural integrity of this complex cytoskeletal domain. Indeed, recent biophysical studies of isolated BBs and cultured epithelial cells demonstrate that Myo1a controls membrane tension by contributing adhesion to the cytoskeleton (Nambiar *et al.*, 2009). Myo1d redistribution along microvilli may rescue membrane tension in KO BBs, but any rescue is expected to be partial because of the lower levels of Myo1d in this structure. Indeed, although a subset of enterocytes in Myo1a KO small intestine exhibit large herniations of BB membrane (Tyska *et al.*, 2005), many cells also demonstrate near normal apical membrane morphology. This mixed population suggests that some enterocytes are able to compensate for the loss of Myo1a. Other recent studies have established that Myo1a plays a critical role in regulating the formation and release of vesicles from microvillar tips (McConnell and Tyska, 2007; McConnell *et al.*, 2009). These studies revealed that Myo1a KO animals produce fewer vesicles that are larger than normal and perturbed in their composition. Thus, microvillar membrane shedding may be a second aspect of Myo1a function that is partially compensated by Myo1d.

CONCLUSION

In this study, we present data establishing Myo1d as a component of the enterocyte BB; these data also suggest that Myo1d may play a role in compensating functions that would otherwise be lost in Myo1a KO mice. The differential localization of these two closely related myosins within individual microvilli and the striking localization of Myo1d to the microvillus tip are likely the result of distinct dynamics and possibly differences in actin-bundle binding affinity. Future studies will investigate the functional role of Myo1d populations in the terminal web and at microvillar tips and explore the detailed mechanism(s) underlying compensation in the Myo1a KO mouse.

ACKNOWLEDGMENTS

The authors thank Chin Chiang (VUMC) and his lab for use of his cryostat, Martin Bahler (Westfälische Wilhelms-Universität Münster, Münster, Germany) for kindly providing a Myo1d antibody, the VUMC Cell Imaging Shared Resource, the VUMC Mass Spectrometry Research Center, and members of the Tyska laboratory for their advice and support. This work was supported by grants from the National Institutes of Health (R01 DK-075555, M.J.T.; R01 CA-126218, D.L.T; P30 DK-058404, and VUMC Digestive Diseases Research Center) and by the American Heart Association (09GRNT2310188, M.J.T.; Predoctoral Fellowship, A.E.B.).

REFERENCES

Bahler, M., Kroschewski, R., Stoffler, H. E., and Behrmann, T. (1994). Rat myr 4 defines a novel subclass of myosin I: identification, distribution, localization, and mapping of calmodulin-binding sites with differential calcium sensitivity. J. Cell Biol. *126*, 375–389.

Belyantseva, I. A., Boger, E. T., and Friedman, T. B. (2003). Myosin XVa localizes to the tips of inner ear sensory cell stereocilia and is essential for staircase formation of the hair bundle. Proc. Natl. Acad. Sci. USA *100*, 13958–13963.

Belyantseva, I. A., Boger, E. T., Naz, S., Frolenkov, G. I., Sellers, J. R., Ahmed, Z. M., Griffith, A. J., and Friedman, T. B. (2005). Myosin-XVa is required for tip localization of whirlin and differential elongation of hair-cell stereocilia. Nat. Cell Biol. *7*, 148–156.

Berg, J. S., and Cheney, R. E. (2002). Myosin-X is an unconventional myosin that undergoes intrafilopodial motility. Nat. Cell Biol. *4*, 246–250.

Cao, Z., *et al.* (2008). Use of fluorescence-activated vesicle sorting for isolation of Naked2-associated, basolaterally targeted exocytic vesicles for proteomics analysis. Mol. Cell Proteom. *7*, 1651–1667.

Chen, Z. Y., Hasson, T., Zhang, D. S., Schwender, B. J., Derfler, B. H., Mooseker, M. S., and Corey, D. P. (2001). Myosin-VIIb, a novel unconventional myosin, is a constituent of microvilli in transporting epithelia. Genomics *72*, 285–296.

Collins, J. H., and Borysenko, C. W. (1984). The 110,000-dalton actin- and calmodulin-binding protein from intestinal brush border is a myosin-like ATPase. J. Biol. Chem. *259*, 14128–14135.

Croce, A., Cassata, G., Disanza, A., Gagliani, M. C., Tacchetti, C., Malabarba, M. G., Carlier, M. F., Scita, G., Baumeister, R., and Di Fiore, P. P. (2004). A novel actin barbed-end-capping activity in EPS-8 regulates apical morphogenesis in intestinal cells of *Caenorhabditis elegans.* Nat. Cell Biol. *6*, 1173–1179.

Fath, K. R., and Burgess, D. R. (1993). Golgi-derived vesicles from developing epithelial cells bind actin filaments and possess myosin-I as a cytoplasmically oriented peripheral membrane protein. J. Cell Biol. *120*, 117–127.

Heintzelman, M.B., Hasson, T., and Mooseker, M. S. (1994). Multiple unconventional myosin domains of the intestinal brush border cytoskeleton. J. Cell Sci. *107*(Pt 12), 3535–3543.

Howe, C. L., and Mooseker, M. S. (1983). Characterization of the 110-kdalton actin-calmodulin-, and membrane-binding protein from microvilli of intestinal epithelial cells. J. Cell Biol. *97*, 974–985.

Hozumi, S., *et al.* (2006). An unconventional myosin in *Drosophila* reverses the default handedness in visceral organs. Nature *440*, 798–802.

Huber, L. A., Fialka, I., Paiha, K., Hunziker, W., Sacks, D. B., Bahler, M., Way, M., Gagescu, R., and Gruenberg, J. (2000). Both calmodulin and the unconventional myosin Myr4 regulate membrane trafficking along the recycling pathway of MDCK cells. Traffic *1*, 494–503.

Kersey, P. J., Duarte, J., Williams, A., Karavidopoulou, Y., Birney, E., and Apweiler, R. (2004). The International Protein Index: an integrated database for proteomics experiments. Proteomics *4*(7), 1985–1988.

Les Erickson, F., Corsa, A. C., Dose, A. C., and Burnside, B. (2003). Localization of a class III myosin to filopodia tips in transfected HeLa cells requires an actin-binding site in its tail domain. Mol. Biol. Cell *14*, 4173–4180.

Matsudaira, P. T., and Burgess, D. R. (1979). Identification and organization of the components in the isolated microvillus cytoskeleton. J. Cell Biol. *83*, 667–673.

McConnell, R. E., Higginbotham, J. N., Shifrin, D. A., Jr., Tabb, D. L., Coffey, R. J., and Tyska, M. J. (2009). The enterocyte microvillus is a vesicle-generating organelle. J. Cell Biol. *185*, 1285–1298.

McConnell, R. E., and Tyska, M. J. (2007). Myosin-1a powers the sliding of apical membrane along microvillar actin bundles. J. Cell Biol. *177*, 671–681.

Mooseker, M. S. (1985). Organization, chemistry, and assembly of the cytoskeletal apparatus of the intestinal brush border. Annu. Rev. Cell Biol. *1*, 209–241.

Mooseker, M. S., and Tilney, L. G. (1975). Organization of an actin filament-membrane complex. Filament polarity and membrane attachment in the microvilli of intestinal epithelial cells. J. Cell Biol. *67*, 725–743.

Nambiar, R., McConnell, R. E., and Tyska, M. J. (2009). Control of cell membrane tension by myosin-I. Proc. Natl. Acad. Sci. USA *106*, 11972–11977.

Salles, F. T., Merritt, R. C., Jr., Manor, U., Dougherty, G. W., Sousa, A. D., Moore, J. E., Yengo, C. M., Dose, A. C., and Kachar, B. (2009). Myosin IIIa boosts elongation of stereocilia by transporting espin 1 to the plus ends of actin filaments. Nat. Cell Biol. *11*, 443–450.

Schneider, M. E., Dose, A. C., Salles, F. T., Chang, W., Erickson, F. L., Burnside, B., and Kachar, B. (2006). A new compartment at stereocilia tips defined by spatial and temporal patterns of myosin IIIa expression. J. Neurosci. *26*, 10243–10252.

Skowron, J. F., Bement, W. M., and Mooseker, M. S. (1998). Human brush border myosin-I and myosin-Ic expression in human intestine and Caco-2BBe cells. Cell Motil. Cytoskelet. *41*, 308–324.

Skowron, J. F., and Mooseker, M. S. (1999). Cloning and characterization of mouse brush border myosin-I in adult and embryonic intestine. J. Exp. Zool. *283*, 242–257.

Speder, P., Adam, G., and Noselli, S. (2006). Type ID unconventional myosin controls left-right asymmetry in *Drosophila.* Nature *440*, 803–807.

Tabb, D. L., Fernando, C. G., and Chambers, M. C. (2007). MyriMatch: highly accurate tandem mass spectral peptide identification by multivariate hypergeometric analysis. J. Proteome Res. *6*, 654–661.

Tyska, M. J., Mackey, A. T., Huang, J. D., Copeland, N. G., Jenkins, N. A., and Mooseker, M. S. (2005). Myosin-1a is critical for normal brush border structure and composition. Mol. Biol. Cell *16*, 2443–2457.

Tyska, M. J., and Mooseker, M. S. (2002). MYO1A (brush border myosin I) dynamics in the brush border of LLC-PK1-CL4 cells. Biophys. J. *82*, 1869–1883.

Tyska, M. J., and Mooseker, M. S. (2004). A role for myosin-1A in the localization of a brush border disaccharidase. J. Cell Biol. *165*, 395–405.

Zhang, B., Chambers, M. C., and Tabb, D. L. (2007). Proteomic parsimony through bipartite graph analysis improves accuracy and transparency. J. Proteome Res. *6*, 3549–3557.